Biophysical Chemistry 144 (2009) 101–107

Contents lists available at ScienceDirect

Biophysical Chemistry

journal homepage: http://www.elsevier.com/locate/biophyschem

Kinetic study of von Willebrand factor self-aggregation induced by ristocetin

Enrico Di Stasio [a], Federica Romitelli [a], Stefano Lancellotti [b], Alessandro Arcovito [a], Bruno Giardina [a], Raimondo De Cristofaro [b,*]

[a] Institute of Biochemistry and Clinical Biochemistry, Catholic University School of Medicine, 00168 Rome, Italy
[b] Hemostasis Research Centre, Institute of Internal Medicine and Geriatrics, Catholic University School of Medicine, 00168 Rome, Italy

ARTICLE INFO

Article history:
Received 11 May 2009
Received in revised form 30 June 2009
Accepted 9 July 2009
Available online 16 July 2009

Keywords:
Protein aggregation
Ristocetin
vonWillebrand factor
Light scattering
Primary haemostasis
Allostery

ABSTRACT

Von Willebrand factor (VWF) is a multimeric glycoprotein present in circulating blood and in secretory granules of endothelial cells and platelets. VWF is sensitive to hydrodynamic shear stress that promotes conformational changes, rendering it able to interact with subendothelial proteins and platelets, thus promoting primary haemostasis. Likewise, the binding of the glycopeptide antibiotic ristocetin to VWF triggers hemostatically relevant conformational transitions. These changes reveal both the interaction site for platelet receptor GpIbα and the Tyr1605-Met1606 peptide bond, which is cleaved by the regulatory metalloprotease ADAMTS-13. In this study we investigated by a combined approach of light scattering spectroscopy and turbidimetry the ability of VWF to self-associate in solution in the presence of ristocetin and in the absence of any protein adsorbing surface. Micro- and macro-aggregates induced by ristocetin, have been characterized under static conditions in the early stage of formation and on a longer time scale (up to 10 h). These findings show that VWF multimers form supramolecular structures favoring platelet trapping not only under high shear stress or interaction with external surfaces, but also in solution under static conditions when the conformational state of the protein is changed only by chemical potential of allosteric effectors.

1. Introduction

Vascular damage is followed rapidly by adhesion and firm attachment of platelets at the site of endothelial injury. At sites of high blood flow, von Willebrand factor (VWF) plays a central role in this process [1,2], as it primarily modulates platelet-subendothelium interaction by linking the platelet receptor GpIb/IX/V to the extracellular matrix [3,4]. In fact, when immobilized on subendothelial matrix, VWF forms a reactive surface capable of capturing platelets from flowing blood [5,6]. High shear stress causes micro- and macro-conformational changes of VWF from a globular state to a stretched chain [7]. VWF derives from a complex gene (180 kb, 52 exons), and is synthesized as pre-pro-VWF, including a 22-residue signal peptide and a 741-residue propeptide. VWF undergoes extensive post-translational processing, glycosylation, and assembly in the endoplasmic reticulum, Golgi and post-Golgi and consists of ~250 kDa monomeric subunits, which form disulfide-linked multimers of 500 to 20,000 kDa. Each VWF subunit contains 2050 amino acids made up of conserved modular domains in the order D8-D3-A1-A2-A3-D4-B1-B2-B3-C1-C2 ([2]). Interaction of the platelet GpIbα receptor with the A1-domain of immobilized VWF [8] results in an initial adhesion, characterized by a continuous surface translocation of the platelets [9]. This process ultimately leads to a stable platelet adhesion through interaction with the platelet collagen receptors GpVI and GpIa/2A [10], activation of the platelet Gp2B/I2A receptor complex [3] and finally to platelet aggregation.

The interaction between VWF and GpIbα does not occur under static conditions and needs a pre-activation of soluble VWF. This process consists of a conformational change of VWF molecules, that expose within the A1 domain the binding site for GpIbα. This mechanism is triggered either by mechanical forces, such as high shear rate (>5000 s^{-1}) found in the arterial circulation, or by chemical potential generated by interaction with external surfaces and chemicals/snake venoms [5,11–15]. Finally, natural mutations causing type 2B von Willebrand disease (VWD 2B) such as the Arg1306Trp or Arg1341Trp [6], are also able to stabilize a conformational state that is prone to the interaction with the platelet receptor even under very low shear conditions and causes platelet clumping in the systemic circulation [6,16].

Recently, it has been demonstrated that VWF multimers undergo a dramatic shape change as a function of shear rate [13,17], which is responsible for the formation of VWF fibers, that are organized as a spider-web like structures. This network may represent an ideal anchor to capture flowing platelets during the process of primary haemostasis [13]. Notably, that VWF could self associate and aggregate

* Corresponding author. Haemostasis Research Center, Dept. of Internal Medicine, Catholic University School of Medicine, Largo F. Vito 1 00167 Rome, Italy. Tel.: +39 06 30156708; fax: +39 06 3015 5915.
E-mail address: rdecristofaro@rm.unicatt.it (R. De Cristofaro).

0301-4622/$ – see front matter © 2009 Elsevier B.V. All rights reserved.
doi:10.1016/j.bpc.2009.07.002

under high shear stress was known from previous studies. For instance, a shear-dependent self-association of VWF in suspension was demonstrated in a cone-plate viscometer [5]. These studies showed that in all cases the aggregation and web-formation process is essentially linked to the mechanical force generated by shear. In this study, we investigated the formation of VWF macro-aggregates induced by ristocetin. The latter is a polyphenol glycopeptide synthesized by the actinomycete *Nocardia lurida*, that was shown to have potent antibacterial activity. The introduction of this antibiotic in clinical practice, caused frequent drug-induced thrombocytopenia, which was demonstrated to be associated with extensive intravascular platelet agglutination [18,19]. Later on in vitro studies discovered that this molecule is able to specifically bind to the A1-domain of VWF, eliciting a conformational change responsible for VWF binding to platelet GpIbα [17]. This property is currently used in the clinical diagnostics of VWD, to detect both defective (type 2A and 2M) and hyper-reactive (type 2B) VWF mutants. The investigation is aimed at assessing the ability of VWF to undergo a self association process induced by chemical potential of this allosteric effector, even in the absence of hydrodynamic shear stress and any protein adsorbing surface.

2. Material and methods

2.1. VWF purification and characterization

VWF was purified from fresh frozen plasma of type A- or B-specific blood group of healthy volunteers by glycine salt precipitation [20]. It was gel filtered on a Sephacryl-S500 3 × 100 column equilibrated with Hepes 10 mM, NaCl 150 mM, pH 7.5 connected to an FPLC apparatus (Pharmacia) operating at a flow rate of 1 ml/min. Eluate was collected in 5 ml-fractions, following the procedure described elsewhere [21]. Electrophoresis and immunoblotting of VWF in 1.5% agarose gels containing sodium dodecyl sulfate (SDS-agarose) was performed as previously described [22]. Final protein concentration was determined by UV absorbance at 280 nm on a double beam Varian model Cary 2200 spectrophotometer (PaloAlto, CA), using an extinction coefficients $\varepsilon_{(0.1\%)} = 0.846$, calculated on the basis of the amino acid composition of the VWF monomer. In addition, VWF concentration was also measured by an immunoturbidometric method, using an automatic coagulometer (Top, Instrumentation Laboratory, Milano, Italy) and a commercially available assay (Hemosyl VWF antigen, Instrumentation Laboratory, Milano, Italy), which show that a concentration of 10 μg/ml VWF, measured by spectrophotometric method, correspond to about 1 U/ml. A modification of the standard protocol for sodium dodecyl sulfate (SDS-agarose) gel was used [22]. After the electrophoresis and immunoblotting of VWF in 1.5% agarose gels, the detection was performed using a chemiluminescence procedure (Amersham Life Science). A sheet of Kodak BioMax MR film (Eastman Kodak Company, New Haven, CT, USA) was placed over the membrane and exposed for times varying from 10 s to 2 min.

Ristocetin (Helena Laboratories Corp., Beaumont, TX) standard solution (16 mg/ml) was prepared and freed of sulphate ions, as previously detailed [23]. The molarity of the ristocetin solution was calculated using a molecular mass value of 2166 Da and an ε value (0.1%, w/v) at 280 nm equal to 4.41. This solution was added to the sample according to the experimental condition under investigation.

2.2. VWF aggregation kinetics induced by ristocetin

2.2.1. Light scattering theory

The outlines of the theory related to light scattering techniques is described in biophysics textbooks [24]. We shall only briefly describe some basic aspects.

2.3. Back scattering measurements

Dynamic Light Scattering (DLS) measurements on protein solutions were carried out with a Zetasizer Nano S (Malvern Instruments, Malvern, U.K.) equipped with a 4 mW He–Ne laser (633 nm). Measurements were performed at 25 °C, at an angle of 173° from the incident beam. Peak intensity analyses were used to determine the average hydrodynamic diameters (*Z*-average diameter) of the scattering particles. Polydispersity index was obtained by a cumulant analysis of the intensity autocorrelation function using version 5.0 of the Nano software [25]. In each measurement the sample was placed in a 45 μl quartz Suprasil cuvette of 10 mm light path (Hellma Italia, Milan, Italy). After the sample was allowed to equilibrate to 25 °C, ristocetin was added and the aggregate formation and evolution was monitored for 24 h. Each measurement was the average of a different number of subruns automatically determined, each being averaged for 10 s. Control measurements were made on solvent and on different ristocetin or VWF concentrations (ranging from 0.01 and 4 mg/ml and 0.01 and 0.9 μM, respectively). Kinetics of the self-aggregation mechanism induced by ristocetin was studied monitoring the *Z*-average diameter and scattered intensity as a function of time. Time zero was defined as a VWF solution in the measurement cell before ristocetin was added.

Both scattered intensity and *Z*-average diameter vs time plots showed a multiphase process. Scattered intensity rapidly increases, reaches a plateau and finally decays (i.e. an asymmetrical bell-shaped curve). On the other hand, the *Z*-average diameter time-dependent profile shows, after an exponential increase (phase 1), a sigmoidal shape. Finally, the asymptote is reached, but significant fluctuation in the *Z*-average diameter values are observed. The process is well described by the following phenomenological equation, that has been used to fit the experimental data according to the least square minimization procedure, by means of Microsoft Excel software:

$$f(t) = R_H^i + \Delta R_1 \times \left(1 - e^{-\frac{t}{\tau}}\right) + \frac{(\Delta R_2)}{\left[1 + \left(\frac{B}{t}\right)^C\right]}$$

where: R_H^i (nm) is the VWF hydrodynamic radius just before the Ristocetin addition and ΔR_1, ΔR_2, B, C and τ are fitting parameters. Moreover, R_H^r (nm) $= R_H^i + \Delta R_1$ is the mean VWF hydrodynamic radius at the end of phase 1, just after Ristocetin addition; and R_H^n (nm) $= R_H^i + \Delta R_1 + \Delta R_2$ is the mean VWF hydrodynamic radius after phase 2. From the analytic function is possible to derive the further following parameters:

1) v_i (nm/min) = the initial rate of the process (i.e., the derivatives at time 0).
2) t_p (min) = the turning point (i.e., the phase 2 starting time — measured by the derivatives sign change).
3) v_m (nm/min) = the maximal rate of phase 2 (i.e., the maximal derivatives).
4) t_m (min) = the v_m corresponding time.

All the derivatives were calculated using a mathematical subroutine of Microsoft Excel Software.

2.4. Turbidimetric measurements

Turbidimetric measurements were performed using DU Series 700 UV/Vis scanning spectrophotometer (Beckman Coulter, Fullerton, CA) selecting the Kinetic/Time mode option. Absorbance at fixed wavelength (350 nm) or spectra (320–700 nm), for a total time of 24 h and reading interval of 1–5 min were recorded. Temperature was set at 25 °C and the sample (prepared as previously described) was transferred in a 45 μl quartz Suprasil cuvette of 10 mm light path (Hellma Italia, Milan, Italy). The kinetics run started immediately after ristocetin was added to the sample. The turbidity of a solution is a

measure of the intensity decrease of transmitted light due to scattering and can be calculated simply by integration of the scattered intensity over all possible directions. Several authors [26,27] have developed theoretical models to determine the size, molecular weight, mass-length ratio of biological macromolecules and systems. Such models were able to describe a reasonable molecular structure when applied to soluble VWF molecules, but completely failed in the analysis of the aggregated system.

3. Results

In Fig. 1 are reported: panel a) a representative SDS-electrophoresis gel and immunoblot for VWF of a sample from normal plasma (A) and purified material (B); panel b) the gel-filtration profile of VWF fractions described by the relative absorbance at 280 nm; panel c) the corresponding hydrodynamic radius R_H and panel d) the polydispersity index from light-scattering measures. For our experiments we pooled fractions 7–13 showing a *Z*-average diameter ranging from of 60 to 80 nm and monomer concentration between 4.0 and 6.5 mg/ml. As expected, the corresponding PDI is in the order of 0.15–0.25 that corresponds to a solution containing a number of particles of different sizes (see Fig. 1 panel b, c and d). This pooled material has been compared by SDS-electrophoresis gel with normal plasma, to demonstrate that the sample used for our kinetic experiments is representative of VWF present under physiological conditions (panel a).

In Fig. 2 are shown the scattered intensities of ristocetin (3 mg/ml) and VWF (0.4 μM) normalized by the same incident intensity (panel a) and the relative distribution intensity (panel c); moreover a concentration dependence of scattered light from ristocetin is shown (panel b). The two molecules appear to be stable with no self-aggregation phenomena occurring over a long span time (~24 h) with VWF/ristocetin scattered light ratio higher than 50; intensity distribution by molecule diameter shows a peak for ristocetin at 2.37 nm (PDI = 0.268) and for VWF at 75.0 nm (PDI = 0.297). We were able to resolve ristocetin peak, as expected by instrument sensitivity, only at concentration >0.5 mg/ml. However, when ristocetin is added to protein solution, VWF strongly dominates the total scattered light at any concentration combination used in the present study.

Representative kinetic profiles of VWF aggregation after addition of ristocetin (VWF 0.4 μM, ristocetin 3 mg/ml, 10 mM Hepes buffer pH 7.0, 5 mM $CaCl_2$ and 125 mM NaCl) are shown in Fig. 3 as a result of two experimental techniques: DLS and turbidimetry. The *Z*-average diameter increase (closed circles) is reported together with the absorbance variation at 350 nm (open circles) over the same time scale, thus showing that during aggregation of this protein, different processes occur. To better clarify this complex mechanism, we first dissected the time course corresponding to the *Z*-average diameter increase.

The VWF mean hydrodynamic radius vs time plot (Fig. 3 closed circles) clearly shows a biphasic profile; in Fig. 4 panel a, the same time course is reported together with the fitted curve using a phenomenological biphasic equation (solid line). In the same picture, we also show the exponential (dashed line) and the sigmoidal part (dotted line) composing the equation used for the fit, as well as the parameters obtained by the fitting procedure according to what explained in the Experimental section. As it is evident, the rapid increase in the *Z*-average diameter, just after ristocetin addition to the solution follows an exponential behaviour that is reminiscent of a diffusion limited reaction leading to formation of aggregates with the R_H raising about 3 fold. This first transition this transition is likely associated with the well-known rapid acquisition of relevant

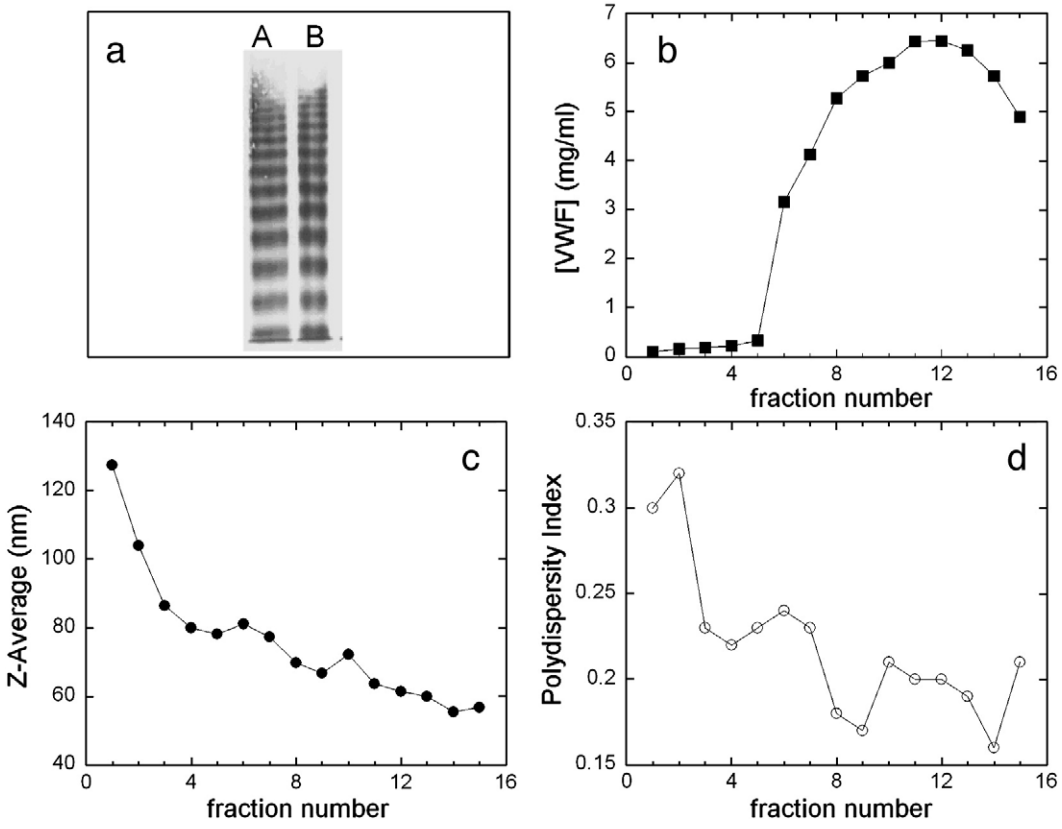

Fig. 1. Panel a) SDS-electrophoresis in 1.5% agarose gel and immunoblot for VWF of a sample from normal plasma (A) and purified material (B). Plasma was diluited 1:50 in 10 mM Tris, 1 mM Na_2EDTA, 2% SDS, pH 8 and 0.005% bromophenol blue as tracking dye. The purified material was used at 20 μg/ml (as monomer) and diluted 1:50 in the above buffer; panel b) gel-filtration profile (■) of VWF fractions described by the relative concentration measured by absorbance reading at 280 nm; panel c) the corresponding *Z*-average diameter (●) and panel d) the polydispersity index (○) determined from light-scattering measures of the same purified fractions.

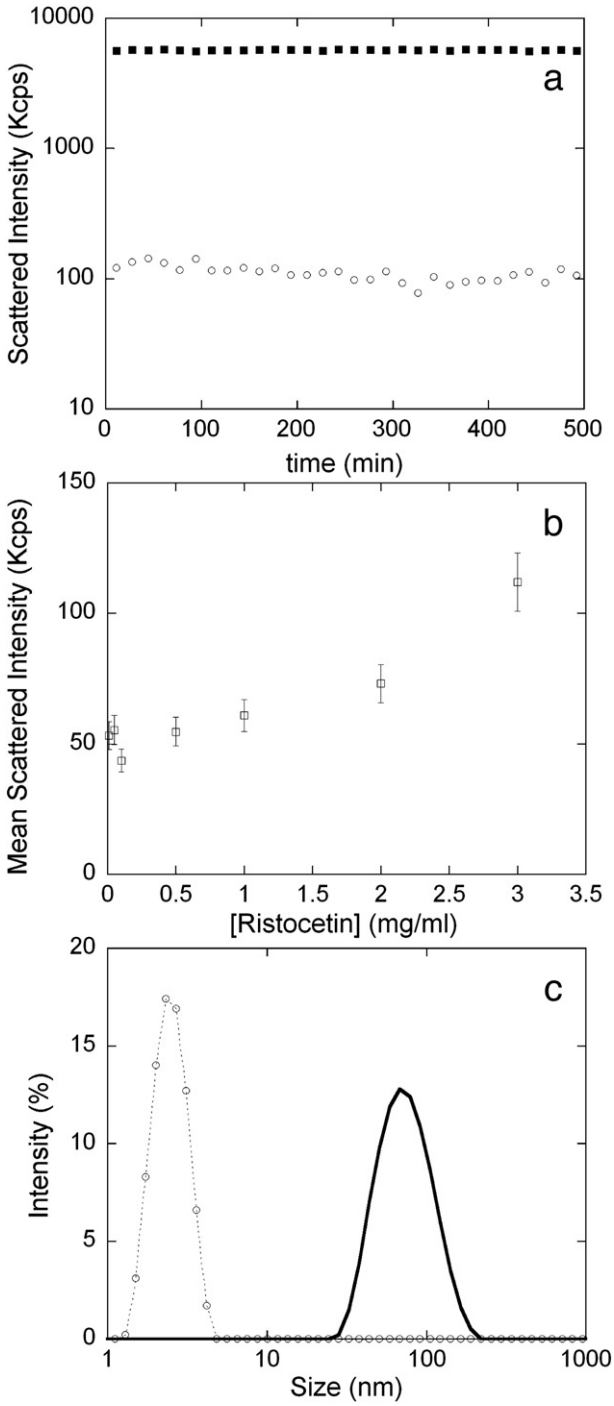

Fig. 2. Panel a) scattered intensities of ristocetin (3 mg/ml — ○) and VWF (0.4 μM — ■) normalized by the same incident intensity (VWF/ristocetin scattered light >50); panel b) scattered light dependence of ristocetin as a function of its concentration and relative standard deviation (□); panel c) intensity distribution as function of molecule diameter. A peak for ristocetin (○) at 2.37 nm (PdI = 0.268) and for VWF (continuous line) at 75.0 nm (PDI = 0.297) was determined. However, ristocetin peak can be resolved only at concentration >0.5 mg/ml so that scattering from VWF strongly dominates the total scattered light from solution of the two molecules at any concentration combination used in the present study.

functional properties such as the enhanced interaction with GpIb and ADAMTS-13 ([18,23]. Subsequently, the time course is well described by a sigmoidal curve and increases the apparent hydrodynamic radius by an order of magnitude. The corresponding scattered intensity (panel b Fig. 4 closed circles) increases until the end of the exponential phase 1, then progressively decreases. This behaviour

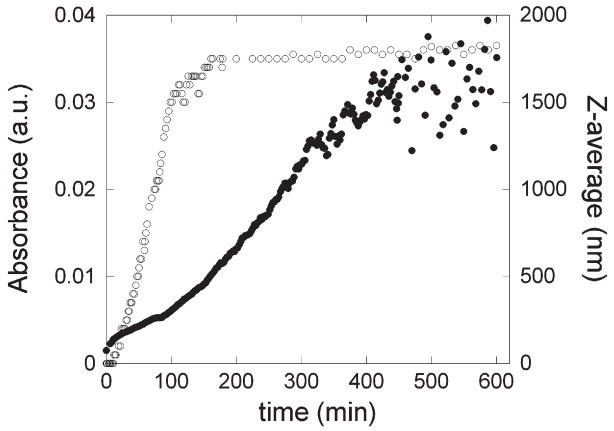

Fig. 3. Time course of VWF aggregation upon ristocetin addition (VWF 0.4 μM, ristocetin 3 mg/ml, 10 mM Hepes buffer pH 7.0, 5 mM $CaCl_2$ and 125 mM NaCl) as detected by *Z*-average diameter variation (●, right ordinate) and absorbance change at 350 nm (○, left ordinate).

can be attributed to destructive interference of larger particles [24]. The polydispersity index (reported in panel b of the same figure) shows values (>0.15), as expected by the intrinsic multimeric state of

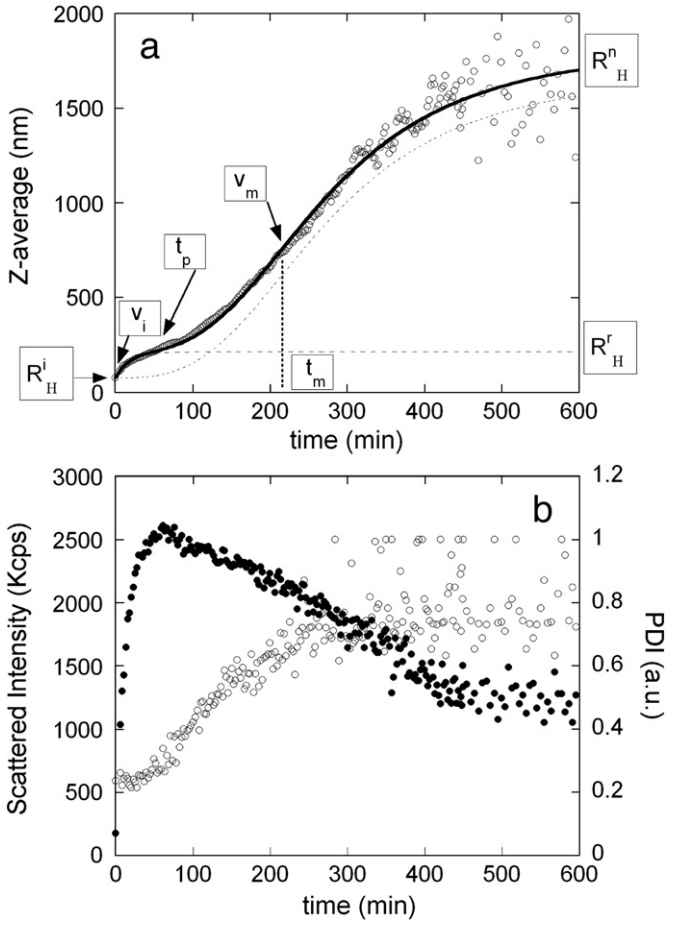

Fig. 4. Panel a) time course of VWF *Z*-Average variation after ristocetin addition (○) (also shown in Fig. 3) is reported together with the fitted curve using the phenomenological biphasic equation decribed in the Materials and Methods section (solid line). The exponential (dashed line) and the sigmoidal part (dotted line) composing the equation used for the fit are shown, as well as the parameters obtained by the fitting procedure (R^i_H (nm) = 75, R^r_H (nm) = 213, R^n_H (nm) = 1844, v_i (nm/min) = 4.45, t_p (min) = 54, v_m (nm/min) = 5.06, t_m (min) = 216); panel b) the corresponding scattered intensity (●, left ordinate) and polydispersity index (○, right ordinate) are reported.

VWF protein. The same index further increases up to 0.8–1.0 during the aggregation process following the kinetic rate constant observed in the corresponding *Z*-average diameter variation. Finally, the significant fluctuation of the asymptotic *Z*-average diameter term at the end of the second phase is indicative of an increase in the heterogeneity of the sample; this condition could be due to the building up of a supra-molecular structure associated with a sol–gel phase transition or the presence of a non-specific protein precipitate. The visual inspection of samples at higher VWF concentrations showed an evident physical phase transition in the absence of any macroscopic precipitate or aggregate thus supporting the first hypothesis.

On the other hand, the absorbance variation reported in Fig. 3 seems to increase following the *Z*-average diameter plot profile until the end of phase 1, then reaches a stable plateau and does not change further during the remainder of the experiment. This behaviour could be related to the cluster dimension (>300 nm) that is reached at the end of the first phase with respect to the incident wavelength (350 nm), that could make it insensitive to further variation.

The effect of ristocetin and VWF concentration on the kinetic process has been further investigated by means of DLS and results are shown in Fig. 5a and b. Addition of ristocetin to VWF solution (0.9 μM) at a final concentration ranging from 0.1 to 1.0 mg/ml is able to quickly increase the R_H to 100–200 nm. However, the *Z*-average diameter vs time profile is limited to phase 1 within 24 h of observation (data not shown). For final ristocetin concentration ≥1.5 mg/ml the previously described two-phase process takes place. An asymptotic R_H of about 400 nm after 3500–4000 min and 800 nm after 1500–2000 min is reached for ristocetin concentration of 1.5 and 2.0 mg/ml, respectively; at higher concentration the apparent final R_H raises to 2000–4000 nm (Fig. 5a). Finally, at a fixed ristocetin concentration of 3 mg/ml, the characteristic multi-steps profile kinetic occurs with each of the single phase being dependent on VWF concentration (range 0.1–0.9 μM, Fig. 5b). As soon as the final plateau is reached for the *Z*-average diameter, its value is insensitive to five fold dilution with a buffer solution containing the same final ristocetin concentration, or to the same dilution with a buffer solution alone (data not shown). This fact demonstrates that the aggregation process is irreversible.

Alternatively, the polymerization-aggregation process can be followed by means of changes of the wavelength (λ) dependence of turbidity (τ) over time. Different theoretical models were described for simple molecule shapes (spheres, rods, random coils [24]). In case of rod-like particles (expected for VWF multimers) with diameters that are small compared with the wavelength, τ should vary as λ^{-3} and should go to zero as $\lambda \to \infty$ [28]. When the fiber diameter grows relative to λ, the plot is no longer linear, but the quantity $c\tau^{-1}\lambda^{-3}$, where *c* is the concentration, changes linearly with λ^{-2}, and the intercept of the plot gives the mass-length ratio of the fibers [27]. This behaviour can be partially observed with soluble VWF molecules (R_H ranging from 35 to190 nm, see Fig. 2c). In the 700–600 nm interval τ/τ_{max} vs λ^{-3} plot is linear (see Fig. 6 — closed circle) but does not extrapolate to the origin (probably due to the presence of particles of different shape arising from the intrinsic multimeric pattern of the protein); for λ ranging from 320 to 600 nm the plot is no longer linear. After addition of ristocetin, the plot completely deviates from the theoretical model and evolves over time progressively deviating from the initial shape, so that the interference at lower wavelength can be only partially ascribed to ristocetin spectroscopic properties. In Fig. 6 we have reported representative curves at intermediate time ($t = 54$ min, open squares) and the time corresponding to the end of the aggregation process ($t = 550$ min, open circles). Finally, the peculiar profile of the plot, not captured by any simple molecular structure model, supports the previously stated hypothesis of a sol–gel phase transition occurring in the sample.

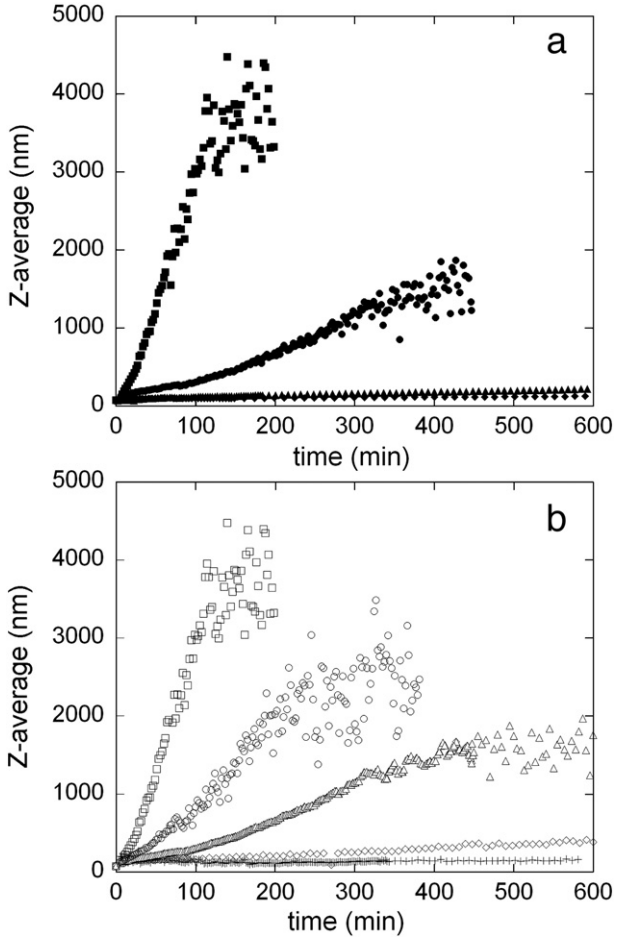

Fig. 5. Panel a) VWF *Z*-average diameter kinetic profile as a function of ristocetin concentration (ristocetin 3(■), 2.5(●), 2(▲) and 1.5(♦) mg/ml, VWF 0.9 μM, 10 mM Hepes buffer pH 7.0, 5 mM $CaCl_2$ and 125 mM NaCl). Panel b) VWF *Z*-average diameter kinetic profile as a function of VWF concentration (VWF 0.9(□), 0.6(○), 0.4(△), 0.2(◇) and 0.1(+) μM, ristocetin 3 mg/ml, 10 mM Hepes buffer pH 7.0, 5 mM $CaCl_2$ and 125 mM NaCl).

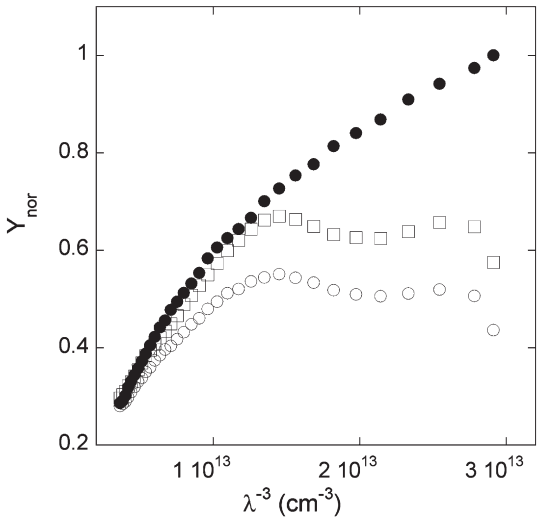

Fig. 6. Ristocetin triggered VWF aggregation process followed by changes of the wavelength (λ) dependence of turbidity (τ) normalized for the maximum value (τ_{max}) over time. $Y_{nor} = \tau/\tau_{max}$ vs λ^{-3} plot of soluble VWF molecules (●) and after addition of ristocetin (□) at $t = 54$ min and at the end of the process (○) at $t = 550$ min. The experimental conditions are the same as indicated in the caption of Fig. 3.

4. Discussion

VWF does not normally interact with platelets in the bloodstream, but exposed vascular subendothelium enables VWF to interact with the platelet glycoprotein Ib–IX–V complex (GP Ib–IX–V). Ristocetin is a poly-phenol molecule, which interacts with the A1 domain of VWF and also promotes interaction of VWF with GPIb–IX–V, thus providing a model for changes in VWF conformation that may occur *in vivo*. The molecular mapping of the ristocetin binding site in the A1 domain of VWF is not known in detail, although site-directed mutagenesis showed some of the residues directly or indirectly involved in binding of the antibiotic (Lys534, Arg571, Lys572, Glu596, Glu613, Arg616, Glu626, and Lys642 of the A1 domain, (numbering based on the A1 primary sequence) [14]). Likewise, the mechanism responsible for the induced conformational changes is not known. Recent X-ray diffraction studies of the GpIb–A1 crystal complex revealed that the α1–β2 loop of A1 serves as a conformational switch. In fact, both an open α1–β2 isomer, which allows faster dissociation of GpIbα–A1, and an extended isomer, which favours tight association, were observed in the complex containing A1 with a wild-type and type 2B von Willebrand Disease (VWD) mutation, respectively [29]. Binding of ristocetin to VWF A1 domain, inducing the interaction of the protein with the N-terminal domain of platelet GpIb, supports the process of primary haemostasis. The latter arises also from the VWF ability to interact with sub-endothelial matrix proteins, such as collagen. Previous studies showed that the transformation of multimeric plasma-derived VWF into a widespread immobilized network depends on several physical and biochemical factors as a critical protein concentration, induced shear stress, and an appropriate anchoring surface, mainly represented in vivo by matrix proteins [13].

In the present study, a multiphase process of VWF conformational transitions after interaction with ristocetin is described for the first time and the kinetic aspect of the reaction are shown. The molecular transition induced *in vivo* by shear stress or promoted *in vitro* by ristocetin is a part of a more complex process composed by different steps. The rapid interaction with ristocetin "activates" VWF molecules triggering an increase in their apparent dimension, as detectable by light scattering measurements. The time course of the first part of the aggregation curve suggests for a diffusion limited process as the maximum aggregate size increases exponentially with time [24]. This process reflects an initial formation of activated clusters of VWF multimers. The second part of the kinetics is characterized by a slower rate constant and by a non exponential time dependence of the increase in the size of the cluster, thus suggesting the occurrence of a reaction-limited regime, culminating with a physical phase transition that is detectable by eye-inspection. We were able to find highly reproducible experimental conditions so that each step of the process can be described. The observed multiphase scattering signal is strongly dominated by the aggregating VWF molecules, even if ristocetin is likely to dimerize at the concentration used in the present study [30]. Ristocetin was previously reported to trigger flocculation of several proteins, included fibrinogen and VWF [30]. However, this process is a non-specific aggregation following a simple linear kinetic. Moreover, in a previous study, the amount of flocculated proteins was evaluated after centrifugation (i.e., after disrupting possible growing supramolecular structures) [30]. We were able to confirm, by light scattering measures, that human fibrinogen flocculation occurs also at low ristocetin concentration (<1 mg/ml — data not shown). On the other hand, the complex kinetic profile observed with VWF, triggered only at high (>1 mg/ml) ristocetin concentration, suggests for a specific binding of molecules and an ordered polymerization process. Finally, the peculiar behaviour of scattered intensity and turbidity could be attributed to destructive interferences by large particles or physical state sol–gel transition as also evident by visual inspection of samples at higher VWF concentrations.

Self-aggregation of VWF was already observed using high hydrodynamic shear stress (>30 dyn/cm^2); in this case the "physical" stretching triggers the molecular activation thus leading to conformational changes promoting the potential adhesion of the protein. Beside inducing the binding to GpIb or to collagen surface, "activated" VWF was demonstrated to self-aggregate [13,31]. However, the data on molecular dimensions of VWF were obtained on the protein studied as a function of shear rate (up to >5000 s^{-1}) in a viscometer and successively transferred in a light scattering apparatus, thus disrupting growing supra-molecular structures. Likewise, a previous study using biotinylated VWF, immobilized on a plastic surface, showed that VWF is able to reversibly self-aggregate under static condition [12]. Both the regions 1–1365 and 1366–2050 are able to inhibit this VWF–VWF interaction [12]. However it must be emphasized that this self-aggregation was obtained under static condition but linked to VWF adhesion to synthetic surface that elicits VWF conformational changes. The present study demonstrates, for the first time, the ability of a chemical potential (i.e., ristocetin binding) to induce in solution under static conditions VWF self-aggregation and network development in suspension, likely mimicking the physiological mechanism, triggered by physical forces, involved in controlling platelet adhesion rates in circulation.

On the basis of the present findings, we propose that the conformational changes induced by ristocetin binding disrupt the multiple domain interactions present in the native VWF structure. Hence, upon stabilization of the extended conformation, the swapped domains of a VWF multimer can interact with another domain of a different multimer. In other words, the non-covalent intramolecular interaction between domains in the same VWF multimer chain, may be broken and restored between different multimer chains by identical intermolecular contacts [32]. This process can contribute to progressive aggregation culminating in a phase transition with the formation of the micro-gel network.

This mechanism, *in vivo*, should optimize the formation of a spider-web like network, which anchors circulating platelets through binding of the GpIb–IX–V membrane complex. Moreover, we can hypothesize that the dimensions of VWF multimers affect the efficiency and thus the rate of this network's formation. The proposed mechanism may play a relevant role in all the clinical conditions characterized by particular abundance of ultra-large VWF multimers such as thrombotic microangiopathies; in fact, a pathological deposition of these VWF aggregates in microcirculation, may contribute to the thrombo-hemorrhagic syndromes occurring in these clinical settings.

Acknowledgements

Financial support by the Italian Ministry of University and Research [Linea D1 "ex-60%" 2007–2008 Università Cattolica Sacro Cuore] and PRIN-2007 [RDC and EDS] are gratefully acknowledged.

References

[1] K.S. Sakariassen, P.A. Bolhuis, J.J. Sixma, Human blood platelet adhesion to artery subendothelium is mediated by factor VIII-von Willebrand factor bound to the subendothelium, Nature 279 (1979) 636–638.
[2] J.E. Sadler, Biochemistry and genetics of von Willebrand factor, Annu. Rev. Biochem. 67 (1998) 395–424.
[3] B. Savage, M. Cattaneo, Z.M. Ruggeri, Mechanisms of platelet aggregation, Curr. Opin. Hematol. 8 (2001) 270–276.
[4] M. Moroi, S.M. Jung, A mechanism to safeguard platelet adhesion under high shear flow: von Willebrand factor-glycoprotein Ib and integrin alphabeta-collagen interactions make complementary, collagen-type-specific contributions to adhesion, J. Thromb. Haemost. 5 (2007) 797–803.
[5] I. Singh, H. Shankaran, M.E. Beauharnois, Z. Xiao, P. Alexandridis, S. Neelamegham, Solution structure of human von Willebrand factor studied using small angle neutron scattering, J. Biol. Chem. 281 (2006) 38266–38275.
[6] J.E. Sadler, U. Budde, J.C. Eikenboom, E.J. Favaloro, F.G. Hill, L. Holmberg, J. Ingerslev, C.A. Lee, D. Lillicrap, P.M. Mannucci, C. Mazurier, D. Meyer, W.L. Nichols, M. Nishino, I.R. Peake, F. Rodeghiero, R. Schneppenheim, Z.M. Ruggeri, A. Srivastava, R.R.

Montgomery, A.B. Federici, Update on the pathophysiology and classification of von Willebrand disease: a report of the Subcommittee on von Willebrand Factor, J. Thromb. Haemost. 4 (2006) 2103–2114.
[7] C.A. Siedlecki, B.J. Lestini, K.K. Kottke-Marchant, S.J. Eppell, D.L. Wilson, R.E. Marchant, Shear-dependent changes in the three-dimensional structure of human von Willebrand factor, Blood 88 (1996) 2939–2950.
[8] S. Miura, C.Q. Li, Z. Cao, H. Wang, M.R. Wardell, J.E. Sadler, Interaction of von Willebrand factor domain A1 with platelet glycoprotein Ibalpha-(1–289). Slow intrinsic binding kinetics mediate rapid platelet adhesion, J. Biol. Chem. 275 (2000) 7539–7546.
[9] B. Savage, E. Saldivar, Z.M. Ruggeri, Initiation of platelet adhesion by arrest onto fibrinogen or translocation on von Willebrand factor, Cell 84 (1996) 289–297.
[10] B. Nieswandt, S.P. Watson, Platelet-collagen interaction: is GPVI the central receptor? Blood 102 (2003) 449–461.
[11] B. Savage, J.J. Sixma, Z.M. Ruggeri, Functional self-association of von Willebrand factor during platelet adhesion under flow, Proc. Natl. Acad. Sci. U. S. A. 99 (2002) 425–430.
[12] H. Ulrichts, K. Vanhoorelbeke, J.P. Girma, P.J. Lenting, S. Vauterin, H. Deckmyn, The von Willebrand factor self-association is modulated by a multiple domain interaction, J. Thromb. Haemost. 3 (2005) 552–561.
[13] A. Barg, R. Ossig, T. Goerge, M.F. Schneider, H. Schillers, H. Oberleithner, S.W. Schneider, Soluble plasma-derived von Willebrand factor assembles to a haemostatically active filamentous network, Thromb. Haemost. 97 (2007) 514–526.
[14] T. Matsushita, D. Meyer, J.E. Sadler, Localization of von willebrand factor-binding sites for platelet glycoprotein Ib and botrocetin by charged-to-alanine scanning mutagenesis, J. Biol. Chem. 275 (2000) 11044–11049.
[15] T. Matsui, J. Hamako, Structure and function of snake venom toxins interacting with human von Willebrand factor, Toxicon 45 (2005) 1075–1087.
[16] E. Groot, P.G. de Groot, R. Fijnheer, P.J. Lenting, The presence of active von Willebrand factor under various pathological conditions, Curr. Opin. Hematol. 14 (2007) 284–289.
[17] M. De Luca, D.A. Facey, E.J. Favaloro, M.S. Hertzberg, J.C. Whisstock, T. McNally, R.K. Andrews, M.C. Berndt, Structure and function of the von Willebrand factor A1 domain: analysis with monoclonal antibodies reveals distinct binding sites involved in recognition of the platelet membrane glycoprotein Ib–IX–V complex and ristocetin-dependent activation, Blood 95 (2000) 164–172.
[18] E.J. Gangarosa, T.R. Johnson, H.S. Ramos, Ristocetin-induced thrombocytopenia: site and mechanism of action, Arch. Intern. Med. 105 (1960) 83–89.
[19] E.J. Gangarosa, N.S. Landerman, P.J. Rosch, E.G. Herndon Jr., Hematologic complications arising during ristocetin therapy; relation between dose and toxicity, N. Engl. J. Med. 259 (1958) 156–161.
[20] I. Ramasamy, A. Farrugia, E. Tran, V. Anastasius, A. Charnock, Biological activity of von Willebrand factor during the manufacture of therapeutic factor VIII concentrates as determined by the collagen-binding assay, Biologicals 26 (1998) 155–166.
[21] H.M. Tsai, Physiologic cleavage of von Willebrand factor by a plasma protease is dependent on its conformation and requires calcium ion, Blood 87 (1996) 4235–4244.
[22] Z.M. Ruggeri, T.S. Zimmerman, The complex multimeric composition of factor VIII/von Willebrand factor, Blood 57 (1981) 1140–1143.
[23] R. De Cristofaro, F. Peyvandi, R. Palla, S. Lavoretano, R. Lombardi, G. Merati, F. Romitelli, E. Di Stasio, P.M. Mannucci, Role of chloride ions in modulation of the interaction between von Willebrand factor and ADAMTS-13, J. Biol. Chem. 280 (2005) 23295–23302.
[24] Schmitz, An introduction to Dynamic Light Scattering by Macromolecules, ACADEMIC PRESS INC, 1990.
[25] D.E. Koppel, Analysis of macromolecular polydispersity in intensity correlation spectroscopy: the method of cumulant, J. Chem. Phys. 57 (1972) 4814.
[26] R.D. Camerini-Otero, R.M. Franklin, L.A. Day, Molecular weights, dispersion of refractive index increments, and dimensions from transmittance spectrophotometry. Bacteriophages R17, T7, and PM2, and tobacco mosaic virus, Biochemistry 13 (1974) 3763–3773.
[27] M.E. Carr Jr., J. Hermans, Size and density of fibrin fibers from turbidity, Macromolecules 11 (1978) 46–50.
[28] E. Casassa, Light scattering from very long rod-like particles and an application to polymerized fibrinogen, J. Chem. Phys. 23 (1955) 596.
[29] J.J. Dumas, R. Kumar, T. McDonagh, F. Sullivan, M.L. Stahl, W.S. Somers, L. Mosyak, Crystal structure of the wild-type von Willebrand factor A1-glycoprotein Ibalpha complex reveals conformation differences with a complex bearing von Willebrand disease mutations, J. Biol. Chem. 279 (2004) 23327–23334.
[30] J.P. Scott, R.R. Montgomery, G.S. Retzinger, Dimeric ristocetin flocculates proteins, binds to platelets, and mediates von Willebrand factor-dependent agglutination of platelets, J. Biol. Chem. 266 (1991) 8149–8155.
[31] S.W. Schneider, S. Nuschele, A. Wixforth, C. Gorzelanny, A. Alexander-Katz, R.R. Netz, M.F. Schneider, Shear-induced unfolding triggers adhesion of von Willebrand factor fibers, Proc. Natl. Acad. Sci. U. S. A. 104 (2007) 7899–7903.
[32] Y. Liu, D. Eisenberg, 3D domain swapping: as domains continue to swap, Protein Sci. 11 (2002) 1285–1299.